NEURAL MODELLING OF ANTISACCADE PERFORMANCE OF HEALTHY CONTROLS AND EARLY HUNTINGTON'S DISEASE PATIENTS

Vassilis Cutsuridis[1,*], Shouyong Jiang[1], Matt J Dunn[2], Anne Rosser[3,4], James Brawn[2], Jonathan T Erichsen[2]

[1]School of Computer Science, University of Lincoln, Lincoln LN6 7TS, UK

[2]School of Optometry and Vision Sciences, Cardiff University, Cardiff CF24 4HQ, UK

[3]Division of Psychological Medicine and Clinical Neurosciences, School of Medicine, Cardiff University, Cardiff, CF14 4XN, UK

[4]Cardiff Brain Repair Group, School of Biosciences, Museum Avenue, Cardiff CF10 3AX, UK

[*]*Corresponding author*

Dr Vassilis Cutsuridis, School of Computer Science, University of Lincoln, Lincoln LN6 7TS, UK. Tel: +44 (0) 1522 83 5107; Email: vcutsuridis@lincoln.ac.uk; ORCID ID: 0000-0001-9005-0260

Abstract

Huntington's disease (HD), a genetically determined neurodegenerative disease, is positively correlated with eye movement abnormalities in decision making. The antisaccade conflict paradigm has been widely used to study response inhibition in eye movements and reliable performance deficits in HD subjects have been observed including greater number and timing of direction errors. We recorded the error rates and response latencies of early HD patients and healthy age-matched controls performing the mirror antisaccade task. HD participants displayed slower and more variable antisaccade latencies and increased error rates relative to healthy controls. A competitive accumulator-to-threshold neural model was then employed to quantitatively simulate the controls' and patients' reaction latencies and error rates and uncover the mechanisms giving rise to the observed HD antisaccade deficits. Our simulations showed: 1) a more gradual and noisy rate of accumulation of evidence by HD patients is responsible for the observed prolonged and more variable antisaccade latencies in early HD; 2) the confidence level of early HD patients making a decision is unaffected by the disease; and 3) the antisaccade performance of healthy controls and early HD patients is the end product of a neural lateral competition (inhibition) between a correct and an erroneous decision process, and not the end product of a third top-down stop signal suppressing the erroneous decision process as many have speculated.

Keywords

Neural model; Antisaccade task; Evidence accumulation; Reaction time; Error rate; Competition

Lead paragraph

Antisaccade task, a behavioral response inhibition paradigm, involves suppression of the reflex to look towards a newly presented target (error prosaccade response) and instead directs the eyes to a position diametrically opposite to target's position (correct antisaccade response). Failure to suppress the error prosaccade response results in a direction error. Two processes usually take place during this task: (1) suppression of an error prosaccade towards the peripheral stimulus, and (2) generation of an antisaccade to the diametrically opposite direction. Participants have been observed to express any of the following three eye movement behaviors during a trial: (1) Participant fails to suppress the error prosaccade resulting in a direction error, (2) Participant makes an antisaccade, or (3) Participant makes an error prosaccade and corrects with a corrected antisaccade in the same trial.

The current accepted dogma in the antisaccade task is that a third top-down inhibitory signal is needed to suppress the error prosaccade in favor of the antisaccade. In line with this dogma past modelling studies of the antisaccade task in health and Huntington disease (HD) required the presence of a third STOP decision signal to suppress in trials the erroneous response. These models although they provided a successful mechanistic view of decision making in the antisaccade task, they failed to capture all aspects of antisaccade performance.

Our research work described in our paper offers an alternative view, which succeeds for the first time to:

1. Capture all aspects of the antisaccade performance of both healthy controls and early HD patients

2. Offer a mechanistic view of processes taking place in the antisaccade paradigm

3. Decipher the mechanisms which give rise to the observed slowed and more variable antisaccade latencies and increased error rates in HD patients relative to healthy controls.

The model shows that the poor HD antisaccade performance is ***not due to*** a deficit in the top-down inhibitory control of the erroneous response as many speculated, ***but instead*** is a product of a competition between two different neuronal populations each coding for a different decision signal: one coding for the erroneous prosaccade decision and the other one for antisaccade decision.

The model accurately reproduces the error rates, response latencies and latency distributions of antisaccades, error prosaccades and corrected antisaccades of both healthy controls and HD participants. Our model also shows that the increased variability in the antisaccade and corrected antisaccade RT distributions of HD participants are due to a slower and noisier accumulation of information (μ and σ), but the HD patients' confidence level required before commitment to a particular course of action is not affected by the disease. Our results have major implications in clinical and pharmaceutical research. Furthermore, our results illustrate the benefits of tightly integrating psychophysical studies with computational neural modelling, because the two methods complement each other and they may provide together a strong basis for hypothesis generation and theory testing regarding the neural basis of decision making in health and in disease.

1 Introduction

HD is a rare, hereditary, neurodegenerative disorder presenting as a mutation in the huntingtin gene (HTT) on chromosome 4p16.3 [1]. The HTT gene contains a trinucleotide cytosine-adenine-guanine (CAG) repeat sequence which in health is below 36 repeats. Expansion above this number leads to the patient developing symptoms, usually in mid-life, although the precise age of onset depends on the length of the CAG repeat expansion (longer repeats are associated with earlier onset of disease) and other genetic factor which are currently only partially understood [2]. Clinically, HD is characterized by motor deficits (including chorea, bradykinesia, dystonia, rigidity, dysarthria, and dysphagia), cognitive deficits, behavioural co-morbidities and eye movement abnormalities [1, 3-8]. The pathophysiology of HD is strikingly selective with atrophy affecting the striatum (caudate and putamen), especially in the early disease stages [9] and external segment of the globus pallidus. Later-on as neurodegeneration becomes more widespread, the brainstem [1, 10-12], thalamus [13-14], and multiple cortical regions [15-17] are also affected. Cortical atrophy in HD begins in posterior regions and progresses anteriorly [18-19].

Eye movement deficits have been well documented in HD. These deficits are more robust in fixation maintenance and voluntary saccade tasks (e.g. antisaccade task) and less in reflexive saccade tasks such as the prosaccade task [20-29]. The response latencies of HD patients were reported to be slower and more variable in the prosaccade task [28-29]. In the antisaccade task, participants, while fixating to a centrally presented target, are instructed to suppress a reflexive saccade (error prosaccade) towards a target presented away from fixation in favor of a saccade to the diametrically opposite position (antisaccade) [30] (see Fig. 1A). While performing a single trial of the antisaccade task any of the following three response types are observed: (1) A direction error when a participant makes just an error prosaccade; (2) A correct response when a participant makes an antisaccade; or (3) A corrected response when a participant makes an error prosaccade and then corrects it with a corrected antisaccade [31-32]. The number and timing of direction errors in the antisaccade task have been reported to be greater in HD patients [28-29].

Modelling studies of the antisaccade paradigm showed for the suppression of an error prosaccade towards the peripheral stimulus in favor of an antisaccade, a STOP process is required [33, 34]. Decision making in these models was a gradual accumulating process till a threshold was crossed and a response was generated. These models consisted of three such accumulator units racing to a threshold: an ANTI unit, a PRO unit, and a STOP unit. The STOP unit prevented the PRO unit from reaching threshold, thus allowing the ANTI unit to reach a different threshold a little later. The authors hypothesized that the threshold level of the PRO unit was higher than the ANTI unit's threshold, reflecting the way the advice was given by the experimenters to every subject to avoid errors. How often the STOP unit cancelled the PRO unit depended on its rate of accumulation (μ) and its variance (σ^2). In the [34] a RESTART mechanism was added to the model [33], such that when the PRO unit reached the threshold first, it restarted the ANTI unit allowing it to reach the threshold and generate the corrected antisaccade response. Both models were successful at capturing aspects of, *but not* the entire antisaccade performance of healthy controls (see [35] for a critique of these two models). Wiecki and colleagues [36] extended the Noorani and Carpenter model without the RESTART mechanism [33] into the realm of early-stage Huntington's disease. The antisaccade reaction time (RT) data of a large cohort of healthy controls, pre-HD and early manifest HD patients from the TRACK-HD study were used [19]. The model simulated accurately the error rates and RT distributions of only the error prosaccades and antisaccades, but not those of the corrected antisaccades of all three participant cohorts.

An alternative approach to simulating the antisaccade paradigm is the Cutsuridis and colleagues series of models [37-41]. In these models, decision making is also a gradual accumulating process till a threshold is crossed, *but only of two* accumulating units: an ANTI unit and a PRO unit (i.e. no STOP unit), which compete one another via lateral inhibition. The Cutsuridis and colleagues models [37-41] have been successful at simulating accurately the *complete* antisaccade performance (error rates and RT distributions of error prosaccades, antisaccades *and* corrected antisaccades) of healthy controls, schizophrenia and obsessive-compulsive disorder patients, while at the same time deciphering the biophysical mechanisms and processes of the antisaccade performances of the three participant cohorts [37, 39-41].

Our current study aims to extend the Cutsuridis and colleagues model [39] in HD by simulating early stage HD antisaccade performance data (reaction times and error rates) in order to understand what causes the observed prolonged and more variable antisaccade latencies and increased error rates in early HD patients relative to healthy controls.

2 Methods

2.1 Experimental data

2.1.1 Sample description

The antisaccade performance (latencies and errors) of 24 healthy controls (18 males, 6 females) (mean age = 48.25; SD = 11.02) and 19 participants (12 males, 7 females) (mean age = 47.74; SD = 12.26) with genetically confirmed HD (presymptomatic to moderately affected) from the South Wales HD Service was recorded. Healthy controls recruited were either Cardiff University students, and/or family members (spouses, partners or gene negative siblings) of HD participants. The investigation was carried out in accordance with the Declaration of Helsinki. The National Health Service Research Ethics Committee for Wales (13/WA/0300) granted approval for this study. All participants gave informed consent. Pregnant women, children younger than age 18, and any participant with a history of neurological disorders other than HD or previous brain injury were excluded from this study. HD participants completed the Unified Huntington's Disease Rating Scale motor examination [49] (total motor score (TMS)), within a three month window prior to eye movement assessment. Table 1 provides the average demographics of both healthy controls and HD participants groups, CAG repeat lengths and mean UHDRS scores of HD participants.

2.1.2 Eye movement task

Participants were seated with the chin supported in a darkened room, 1 m from a 70″ rear projection screen. Eye movements were recorded at 1000 Hz using an EyeLink 1000+ eye tracker (SR Research, Ottawa, Ontario, Canada). A five-point calibration was performed using the built-in calibration

procedure [50]. During the antisaccade task, a single 1° red fixation target was shown at all times in the form designed by Thaler et al. [51] on an otherwise dark screen. An antisaccade trial began with the target in the screen centre for a random duration of 1000–1500 ms. The target then stepped to one of six peripheral locations (±5°, ±10° and ±15°) where it remained for a random duration between 1000–1500 ms. Possible target positions were not cued in any way. The target then stepped back to the screen centre, and the next trial began immediately. Each target location was repeated 16 times, and the order of presentations within paradigms was randomized. Prior to the start of the task, the experimenter explained the task until participants confirmed they understood the instructions. Participants were instructed to look at the target while in the central position and then to look to the exact mirror image location of the peripheral target as fast and accurately as possible.

2.2 Eye movement recording and analysis

Any samples reporting a gaze position ≥ 50% beyond the screen edge were discarded as artefacts. Short gaps in the data (≤ 25 ms) were interpolated with cubic splines. Any remaining data lying ≥ 10 standard deviations from the median gaze position for the entire recording were discarded as artefacts. Next, to remove remaining blink-related artefacts, all data ≤ 75 ms either side of all gaps in the data were also deleted. Position data were then filtered using a generalized Savitzky-Golay filter, as described by [52].

Saccades were detected using the method described by Engbert and Kliegl [53]. For each target jump, the saccade most likely to represent the participant's response was determined by selecting the first saccade in the axis of the target jump occurring between 100 and 1000 ms following the jump with an amplitude within 50-400% of the amplitude required to land in the correct antisaccade position. Trials with latencies less than 100 ms were considered as anticipations and thus were excluded. Trials with latencies greater than 1000 ms were also excluded because they were considered as trials where participants lost interest or were bored. The onset time of this saccade (relative to the target jump) defined the reaction time (RT) for the trial. Depending on the direction of this saccade, it was labelled as an 'antisaccade' or an 'error prosaccade'. If an error prosaccade was subsequently corrected by an

antisaccade, then this movement was regarded as a 'corrected error prosaccade'. Figures 1B & 1C depict traces of error prosaccade, antisaccade and corrected antisaccade trajectories.

Trials containing dropped data (i.e. due to blinks) were excluded from analysis. Between each trial, the landing position of the return-to-center prosaccade was used to drift-correct subsequent position data, unless the centripetal prosaccade landed $\geq 2°$ away from that of the previous trial.

2.3 Neural network model

A one-layer competitive neural network consisting of N rate nodes was employed (Fig. 2A). The complete mathematical description of the model can be found in [39]. To assist the readers of this paper and increase our article's readability we provide below a brief description of the model's architecture and inputs. The left half network coded for the error decision signal, whereas the right half one coded for the correct decision signal. All nodes in the network model were connected via short-range lateral excitation and long-distance lateral inhibition. In the left half of the network the inverse of the integration time constant, τ^{-1}, took values from a normal distribution with mean (μ_1) and standard deviation (σ_1), whereas in the right half τ^{-1} took values from a different normal distribution with mean (μ_2) and standard deviation (σ_2) (see Table 2 for values). The connectivity matrix w_{ij} between nodes was a shifted Gaussian kernel, which depended only on the spatial distance between nodes, and it was excitatory for neighbouring nodes to the node activated by the input and inhibitory for distant ones (Fig. 2B) [41].

Network nodes were activated by an (exogenous) reactive input (I_r) representing the error decision signal (error prosaccade) and an (endogenous) planned input (I_p) representing the correct decision signal (antisaccade). The exogenous input activated a randomly selected node and two of its closest neighbors on each side of it, whereas the endogenous input activated the mirror node and its two nearest neighbor nodes on each side of it. The endogenous input was considered to be stronger than the exogenous one ($I_p > I_r$; see Table 2 for values). A 50 ms presentation delay between the inputs was also considered with the exogenous input been presented first followed by the endogenous one. Both inputs remained active for 1000 ms.

2.3.1 Model calibration

The model had five key parameters (parameters μ_1, σ_1, μ_2, σ_2, T_h from Table 2) which needed to be optimised to fit the data. To carry out optimisation, we first defined a single-objective function that minimised the squared error between our model prediction and experimental data:

$$f = \sum\left(\frac{x_{e,i}-x_{c,i}^{exp}}{\bar{x}_e^{exp}}\right)^2 + \sum\left(\frac{x_{a,i}-x_{a,i}^{exp}}{\bar{x}_a^{exp}}\right)^2 + \sum\left(\frac{x_{c,i}-x_{c,i}^{exp}}{\bar{x}_c^{exp}}\right)^2 \quad (1)$$

where $x_{k,i}$, $x_{k,i}^{exp}$ were respectively the simulated and experimental values at time point i for activity k, with k being either `e' (error prosaccades), `a' (antisaccades), or `c' (corrected antisaccades). $\bar{x}_k^{exp}$ was the average experimental value for activity k used to normalise the data so that the three activities were equally treated in optimisation. The algorithm chosen to minimise the objective function was the particle swarm optimisation (PSO) algorithm [54], a nature-inspired global optimisation algorithm that makes use of swarm intelligence to guide the search toward optima. PSO did not rely on gradient information and was well suited to our simulation optimisation. We used the standard PSO with a population size of 50 in MATLAB to perform the optimisation. The algorithm was run for a maximum generation of 100. Best solutions from 10 runs were obtained for controls and HD. Due to the stochastic nature of the model, we took the average of 30,000 trials as the objective value for each solution evaluation.

2.4 Data analysis

For the analysis of our experimental and simulation-generated data we replicated the data and statistical analysis measures of Cutsuridis and colleagues' study [39]. To assist our readers and increase the readability of our manuscript, we provide below a brief description of these measures. Experimental saccade latency was measured from the peripheral stimulus onset till the onset of the first detectable eye movement (see Figure 1). Simulated saccade latency was measured as the time interval between the

onset of the (exogenous) reactive input till the time the activity of the model neurons reached the threshold (parameter T_h in Table 2) plus an experimentally reported 30ms conduction latency required for the motor decision to reach the eye muscles [55]. Experimental and simulated latencies for healthy controls and HD patients were further divided into: (1) error prosaccades, (2) antisaccades, and (3) corrected antisaccades (see Figure 1).

For the experimental latencies the median and coefficient of variation (CV) values for the error prosaccades, antisaccades and corrected antisaccades were calculated for each participant (24 controls and 19 HD patients). In a similar fashion for the simulated latencies the median and CV values for the error prosaccades, antisaccades and corrected antisaccades were calculated for each simulated subject (control subject vs patient subject). Because both the experimental and simulation-generated data were not normally distributed, CV was calculated as the quotient of the inter-quartile range (third quartile (Q_3) – first quartile (Q_1)) divided by the median latency. A Mann-Whitney U test was subsequently employed to compare the group median distributions of the experimental and simulated controls and HD patients.

For the average cumulative percent probability distribution function for the error prosaccades, antisaccades and corrected antisaccades we organized the latencies for each participant in ascending order and calculated the quantile values at 1%, 2%, 5%, 10%, 20%, 30%, 40%, 50%, 60%, 70%, 80%, 90%, 95%, 98%, 99.9% (15 bins in total). The quantile values were then averaged across each response group to give the average group quantile values for error prosaccades, antisaccades and corrected antisaccades. It has been shown that the average distribution retains the basic shape characteristics of the individual distributions [56]. To test the difference between the group response and participant distributions, a Wilcoxon signed rank test (*signrank* function in MATLAB) was utilized.

Each cumulative latency value was then inverted (i.e. 1/latency) and plotted in a reciprobit plot, which resulted into latencies falling on a straight line [57]. A best-fitting regression line for each group using the regression coefficients that our model produced was computed and an R correlation coefficient was estimated to assess how good fit was the simulated regression line to the experimental data. Finally, a comparison of the two simulated regression lines for the patient and control groups using the

homogeneity of slopes and intercepts regression analysis was performed as described in Weaver and Wuensch study [58].

3 Results

3.1 Experimental latencies

The median inter-participant value of the median intra-participant RT for the error prosaccades was 201 ms (Q_1 = 183.5 ms, Q_3 = 224 ms, inter-quartile range (IQR) = 41 ms) for the healthy controls and 210 ms (Q_1 = 191 ms, Q_3 = 234 ms, IQR = 43 ms) for the early HD patients (Fig. 3; see Table 3). Their 9 ms difference was not statistically significant (Z = -0.9889, P = 0.3227). The CV of the error prosaccade RTs for the healthy controls was calculated to be 0.1674, whereas for the patients was 0.1989 (see Table 4).

Histograms of the RT distributions are usually more greatly skewed in patients than in healthy controls, indicating a larger RT variability. To test whether that was also the case in our data an average cumulative RT distribution for each group (controls vs. patients) was computed as described in section "2.4 – Data analysis". To test the difference between the group distributions for patients and controls, a Wilcoxon signed rank test was used. The two cumulative error prosaccade RT distributions (see Fig. 4 top) did not differ in shape (P = 0.0915).

Similar analysis measures were used for the antisaccades and corrected antisaccades for both the controls and HD patients. The median inter-participant value of the median intra-participant RT for the antisaccades was 291.5 ms (Q_1 = 257 ms, Q_3 = 338 ms, IQR = 81 ms) for the controls and 329.75 ms (Q_1 = 294.25 ms, Q_3 = 405.63 ms, IQR = 111.38 ms) for the HD patients (Fig. 3; see Table 3). Their 38.25 ms difference was statistically significant (Z = -2.7121, P = 0.0067). The CV of antisaccade RT was 0.2956 for the controls and 0.3251 for the patients (see Table 4).

The average cumulative antisaccade RT distribution for each group (controls vs. patients) was computed as before. The average cumulative antisaccade RT distribution curve for the patients

consisted of an early and a late component (see Fig 4 middle). A Wilcoxon signed rank test testing for the difference between the two group distributions showed they were not different in shape (P = 0.3514). When the late component of the average cumulative RT distribution of the patients was compared with the average cumulative RT distribution of the healthy controls, then these two cumulative distributions were found to significantly differ in shape ($P < 10^{-4}$).

Finally, the median inter-participant value of the median intra-participant RT for the corrected antisaccades was 429 ms (Q_1 = 363.5 ms, Q_3 = 466 ms, IQR = 102.5 ms) for the controls and 480 ms (Q_1 = 413 ms, Q_3 = 553.25 ms, IQR = 140.25 ms) for the HD patients (Fig. 3; see Table 3). Their 51 ms difference was statistically significant (Z = -2.5603, P = 0.0105). The CV value of corrected antisaccade RT was 0.2665 for the controls and 0.2667 for the patients (see Table 4).

A Wilcoxon signed rank test testing for the difference between the group cumulative corrected antisaccade RT distributions for patients and controls showed they differed in shape (see Fig 4 bottom) and this difference was significant ($P < 10^{-3}$).

3.2 Experimental versus simulated latencies

3.2.1 Controls

We run the model for 30,000 trials in each trial recording the latency of the generated response (error prosaccade or antisaccade or corrected antisaccade). The model parameters we chose to vary into order to fit the model data to the experimental data were: (1) the inverse of the integration constants, τ^{-1} of the nodes coding for the error and correct decision signals, and (2) the threshold, T_h. Our choice of the particular parameters to vary was based on previous parametric investigation of the first author in [39], which showed that variability in interneuronal distance, or input strength, or network size, or in background noise did not produce the latency distributions of error prosaccades, antisaccades and corrected antisaccades. In this study, we considered in each trial run each τ^{-1} to take values from a different normal distribution with mean μ and standard deviations σ. As we described in section "2.4 – Data analysis" the model error prosaccade reaction time was estimated as the time interval from the

onset of the exogenous input (reactive input, I_r) until the time the activity of the node coding for the reactive input crossed T_h plus an additional 30 ms (Fig. 2C). Similarly, the antisaccade and corrected antisaccade reaction times were estimated as the time intervals from the onset of the exogenous input (reactive input, I_r) until the time the activity of the node coding for the planned input crossed T_h plus 30 ms (Fig. 2C). The antisaccade was flagged as the trial when only the neuronal activity of the node coding for the endogenous input (planned input) crossed T_h. The corrected antisaccade was flagged as the trial when both the neuronal activities of the nodes coding for the endogenous (planned) and exogenous (reactive) inputs crossed T_h.

Variation of the τ^{-1} (μ and σ) for both nodes integrating the reactive (μ_1 and σ_1) and planned (μ_2 and σ_2) inputs (see Table 2 for parameter values used in the control cohort) produced the following results: The simulated median controls RTs for the error prosaccades, antisaccades and corrected antisaccades were 204.7 ms (Q_1 = 183.29 ms, Q_3 = 230.88 ms, IQR = 47.59 ms), 286.84 ms (Q_1 = 258.02 ms, Q_3 = 323.55 ms, IQR = 65.53 ms) and 438.55 ms (Q_1 = 377.84 ms, Q_3 = 519.89 ms, IQR = 142.05 ms), respectively (Fig 5; see Table 3). As we reported in section "3.1 – Experimental latencies" the experimental healthy controls RTs for the error prosaccades, antisaccades and corrected antisaccades were 201 ms (Q_1 = 183.5 ms, Q_3 = 224 ms, IQR = 41 ms), 291.5 ms (Q_1 = 257 ms, Q_3 = 338 ms, IQR = 81 ms), and 429 ms (Q_1 = 363.5 ms, Q_3 = 466 ms, IQR = 102.5 ms), respectively (Fig 4; see Table 3). The 3.7 ms difference between the experimental and simulated error prosaccades RT was not found to be statistically significant (Z = 0.132, P = 0.8947). Similarly, the 4.66 ms difference between the experimental and simulated antisaccades RT was not statistically significant (Z = -0.0698, P = 0.9444) and so was the 9.55 ms difference between the experimental and simulated corrected antisaccades RT (Z = -1.8468, P = 0.0648).

The simulated healthy controls' CVs for the error prosaccades, antisaccades and corrected antisaccades were found to be 0.2325, 0.2285 and 0.3239, respectively, whereas the CVs for the experimental controls' error prosaccades, antisaccades and corrected antisaccades were 0.1674, 0.2956, 0.2665, respectively (see Table 4).

Comparison of the experimental and simulated average cumulative RT distributions for error prosaccades, antisaccades and corrected antisaccades with a Wilcoxon signed rank test showed that the shapes of the experimental and simulated cumulative distributions of the error prosaccades ($P = 0.5245$), antisaccades ($P = 0.5614$) and corrected antisaccades ($P = 0.012$) did not differ in shape. Transformation of each average cumulative RT distribution in a reciprobit scale and best-fit of the simulated data (regression line) to the experimental data (data points) for each response type (error prosaccades, antisaccades and corrected antisaccades) resulted in the following mean squared error values: 3.4221e-8 (error prosaccades), 9.7607e-9 (antisaccades), 4.7717e-8 (corrected antisaccades). The correlation coefficient R value for all three response types was 0.99 (see right plots of Figs. 8 top, 8 middle, and 8 bottom).

Clearly from these statistical analysis results, the model faithfully represented the healthy controls cohorts's error prosaccades, antisaccades and corrected antisaccades responses properties (medians, variabilities, and distribution shapes).

3.2.2 HD patients

As before, to fit the simulated HD data to the experimental ones, we ran the model for 30,000 trials, in each trial varying the threshold T_h and the inverse of the integration constants, τ^{-1} (μ and σ) of the nodes coding for the error (μ_1 and σ_1) and correct (μ_2 and σ_2) decisions (refer to Table 2 for these parameter values). The simulated median HD RTs for the error prosaccades, antisaccades and corrected antisaccades were 211.1 ms (Q_1 = 183.63 ms, Q_3 = 248.79 ms, IQR = 65.16 ms), 324.35 ms (Q_1 = 281.08 ms, Q_3 = 383 ms, IQR = 101.92 ms) and 497.9 ms (Q_1 = 421.51 ms, Q_3 = 580.2 ms, IQR = 158.69 ms), respectively (Fig 6; see Table 3). The experimental median HD RTs for the error prosaccades, antisaccades and corrected antisaccades were 210 ms (Q_1 = 191 ms, Q_3 = 234 ms, IQR = 43 ms), 329.75 ms (Q_1 = 294.25 ms, Q_3 = 405.63 ms, IQR = 111.38 ms), and 480 ms (Q_1 = 413 ms, Q_3 = 553.25 ms, IQR = 140.25 ms), respectively (Fig 6; see Table 3). The 1.1 ms difference between the experimental and simulated error prosaccades RT was not statistically significant ($Z = 0.5261$, $P = 0.5988$). Similarly, the 5.40 ms difference between the experimental and simulated antisaccades RT

was not statistically significant (Z = 1.3722, P = 0.17). The 17.9 ms difference between the experimental and simulated corrected antisaccades RT was also not statistically significant (Z = -0.0635, P = 0.9494).

The simulated HD CVs for the error prosaccades, antisaccades and corrected antisaccades were 0.3183, 0.3553 and 0.3618, respectively, whereas the CVs for the experimental HD error prosaccades, antisaccades and corrected antisaccades were 0.1989, 0.3251, 0.2667, respectively (see Table 4).

When we compared the simulated and experimental average cumulative RT distributions of each response type, we found their shapes did not differ (Error prosaccades: P = 0.5614; Antisaccades: P = 0.6387; Corrected antisaccades: P = 0.7615). As before transformation of each average cumulative RT distribution in a reciprobit scale and best-fit of the simulated data (regression line) to the experimental data (data points) for each response type resulted in different, but still low mean squared error values: 2.0279e-7 (error prosaccades), 1.4622e-6 (antisaccades), 1.8441e-8 (corrected antisaccades). The correlation coefficient R value for all three response types (error prosaccades, late component of antisaccades, and corrected antisaccades) was found once again to be 0.99 (see right plots of Figs. 8 top, 8 middle, and 8 bottom).

Clearly from these statistical analysis results, the model faithfully represented each HD patient cohort's response properties (medians, variabilities, and distribution shapes).

3.3 Simulated controls versus simulated HD patient latencies

When we compared and contrasted the simulated healthy controls and simulated HD data we found the following: The median RT value of the error prosaccades, antisaccades and corrected antisaccades for the simulated healthy controls were 204.7 ms (Q_1 = 183.29 ms, Q_3 = 230.88 ms, IQR = 47.59 ms), 286.84 ms (Q_1 = 258.02 ms, Q_3 = 323.55 ms, IQR = 65.53 ms) and 438.55 ms (Q_1 = 377.84 ms, Q_3 = 519.89 ms, IQR = 142.05 ms), respectively (Fig 7; see Table 3). The median RT value for the error prosaccades, antisaccades and corrected antisaccades for the simulated HD patients were 211.1 ms (Q_1 = 183.63 ms, Q_3 = 248.79 ms, IQR = 65.16 ms), 324.35 ms (Q_1 = 281.08 ms, Q_3 = 383 ms, IQR = 101.92 ms) and 497.9 ms (Q_1 = 421.51 ms, Q_3 = 580.2 ms, IQR = 158.69 ms), respectively (Fig 7; see Table 3). The 6.4 ms difference between the median error prosaccade RT values of the simulated healthy

controls and simulated HD was found to be statistically significant ($Z = -12.86$, $P < 10^{-3}$). Similarly, the 37.51 ms difference between the median antisaccade RT values simulated healthy controls vs simulated HD patients was statistically significant ($Z = -49.94$, $P = 0$) and so was the 59.35 ms difference between median corrected antisaccade RT values ($Z = -28.4$, $P < 10^{-3}$).

A Wilcoxon signed rank test tested the shape difference of the two error prosaccade cumulative distributions of the two participant cohorts and found it not statistical significantly different ($P = 0.073$) (see left plot of Fig 8 top). However, the shape difference of the two antisaccade cumulative distributions was statistically significant ($P < 10^{-3}$) as was the difference for the corrected antisaccades ($P < 10^{-3}$) (see left plots of Fig 8 middle and 8 bottom).

When we extracted the coefficients (slope and intercept) of each best-fitted regression line (simulated data) to the data points (experimental 1/RT data) (see right plots of Fig 8 top, middle and 8 bottom) a comparison of the homogeneity of slopes showed that both (controls and patients) fitted error prosaccade, antisaccade and corrected antisaccade lines were not different in slope (Error prosaccade: $t_{26} = 0.1866$, $p = 0.853423$; Antisaccade: $t_{26} = 0.0542$, $p = 0.95719$; Corrected antisaccade: $t_{26} = 9.8377e\text{-}04$, $p = 1$). However, a comparison of intercepts homogeneity showed controls and patients fitted error prosaccade, antisaccade and corrected antisaccade lines were significantly different in intercept (Error prosaccade: $t_{26} = 6598$, $p < 10^{-4}$; Antisaccade: $t_{26} = 2986$, $p < 10^{-4}$; Corrected antisaccade: $t_{26} = -265.3327$, $p < 10^{-4}$).

3.4 Errors

Two types of direction errors were observed in the experimental data: (1) A corrected direction error when a participant made an error prosaccade followed by a corrected antisaccade in the same trial, and (2) An uncorrected direction error when a participant made just an error prosaccade towards the peripheral stimulus. Experimental error rate was calculated as the total number of corrected and uncorrected direction errors divided by the total number of responses. In the two participant cohorts we tested, 23% of the total responses were errors in healthy controls, whereas 61.82% of the total responses

were errors in early HD patients (see also Table 3). Similarly, the errors in the simulation generated data were of two types: (1) Corrected errors, and (2) Uncorrected errors. An uncorrected model error was when only the activity of the node coding for the exogenous input (error prosaccade) crossed the threshold, whereas a corrected model error was when the activity of the node coding for the exogenous input crossed the threshold followed by the activity of the node coding for the endogenous input. The estimated total model error (uncorrected + corrected errors) rate was 31.13% for the simulated healthy controls and 62.23% for the simulated early HD patients (see Table 3).

4 Discussion

A number of questions present themselves. Why even early stage HD patients perform so poorly in the antisaccade task? Why early stage HD patients' response latencies are so much slower and more variable than those of healthy controls? Why early stage HD patients make more wrong decisions than controls? Our modelling study has provided answers to these important questions. First of all, our study showed the level of confidence for making a decision (decision threshold level, T_h, in Table 2) by both participant cohorts (controls vs early stage HD patients) was the same. But where in the brain is the decision threshold level set? Many have suggested in the basal ganglia structures [42]. The HD pathophysiology is strikingly selective with atrophy affecting the basal ganglia (BG), particularly the striatum (caudate and putamen) [9] and external segment of the globus pallidus. Our simulation results showed BG in early stage HD is potentially unaffected by the disease since the decision threshold level (T_h) does not change in early stage HD patients.

Furthermore, our study showed the decision centres of early stage HD patients are more noisy than those of healthy participants. The noise is more prominent in the rate by which decision making neurons accumulated information (μ and σ) towards a fixed threshold (level of confidence). The value of μ_2 (see Table 2) is greater in the control condition than in HD condition implying that antisaccades and corrected antisaccades are slower in early stage HD than in health. Similarly, σ_2 value (see Table 2) is smaller in the control condition than in HD condition implying that antisaccade and corrected

antisaccade latencies are more variable in HD patients than in healthy participants. In [43] first author has showed a potential neurophysiological correlate of a variable rate of evidence accumulation τ^{-1} is variability in NMDA receptor conductance. Experimental studies have shown that cortical and striatal NMDA dysfunction maybe implicated in HD in transgenic HD mice [44]. These results might have important implications in clinical and pharmaceutical research. The focus of clinical research has shifted towards early intervention to slow the disease progression, which requires detection of subtle cognitive changes before the symptoms become neurologically apparent. As of today, there are no such clinically approved therapies that can reverse the cognitive decline of HD patients. However, a clinical drug targeting NMDA receptors in a concentration dependent way may be a way to alleviate some of the HD symptoms related to cognitive decline.

There is yet another question our simulation study successfully addresses: Is a third independent top-down STOP signal necessary to stop an erroneous prosaccade after an correct antisaccade has been generated first? Such a STOP signal has been utilized in few computational modelling studies [33-34], but no one has so far been able to record it experimentally. Few speculated the origins of such a STOP signal may be the prefrontal cortical and/or basal ganglia structures [32, 45]. A recent computational study investigating the antisaccade performance of healthy controls, pre-HD and early manifest HD participants has suggested that such a STOP process is necessary to suppress the error prosaccade that would otherwise be generated [36]. By incorporating such a STOP signal into their model, they successfully simulated the latency distributions of only error prosaccades and antisaccades, *but not* those of the corrected antisaccades [36]. On the other hand, our simulation study *for the first time* provided evidence that the presence of a third inhibitory STOP process is not necessary at least in early stage HD, but instead competition between the PRO and ANTI decision neurons encoding for the error prosaccade and antisaccade decision signals, respectively, is sufficient to stop at all trials the error prosaccade from crossing the threshold when the antisaccade has crossed it first. In contrast to [36] our model was able to simulate accurately *all aspects* of the antisaccade performance of *both participant cohorts*, namely the error prosaccade, antisaccade and corrected antisaccade latency distributions as well as their error rates.

Overall, our computational neural modelling study tightly coupled with psychophysical eye tracking recordings in health and disease provides a novel general framework for generation and testing of hypothesis in neural decision making.

Acknowledgements

VC conceived, developed and implemented the model, performed statistical and data analysis, and wrote the paper. SJ performed statistical and data analysis. MD and JE conceived the experimental paradigm and designed the experimental protocol. MD wrote the experimental data section of the paper. JB carried out the psychophysical experiments and collected the data. AR recruited the HD participants. JE and AR proofread the paper. VC is grateful to MD, JE, JB and AR for sharing their healthy controls and early HD eye movement datasets with him. VC is also grateful to SJ for running the additional model calibration simulations. The authors declare that they have no competing financial interests.

Data availability statement

Data are available upon request to JE

References

[1] Rüb, U., Hoche, F., Brunt, E. R., Heinsen, H., Seidel, K., Del Turco, D., et al., "Degeneration of the cerebellum in Huntington's Disease (HD): possible relevance for the clinical picture and potential gateway to pathological mechanisms of the disease process," Brain Pathol 23, 165–177 (2013).

[2] Ghosh, R., and Tabrizi, S. J., "Clinical Features of Huntington's Disease," Adv Exp Med Biol 1049, 1-28; 10.1007/978-3-319-71779-1_1 (2018).

[3] Walker, F. O., "Huntington's disease," Semin Neurol 27, 143–150 (2007a).

[4] Walker, F. O., "Huntington's disease," Lancet 369, 218–228 (2007b).

[5] Lasker, A.G., and Zee, D. S., "Ocular motor abnormalities in Huntington's disease," Vision Res 37(24), 3639–45 (1997).

[6] Grimbergen, Y. A., Knol, M. J., Bloem, B. R., Kremer, B. P., Roos, R. A., and Munneke, M., "Falls and gait disturbances in Huntington's disease," Mov Disord 23, 970–976 (2008).

[7] Busse, M. E., Wiles, C. M., and Rosser, A. E., "Mobility and falls in people with Huntington's disease," J Neurol Neurosurg Psychiatry 80, 88–90 (2009).

[8] Rüb, U., Heinsen, H., Brunt, E. R., Landwehrmeyer, B., Den Dunnen, W. F., Gierga, K., and Deller, T., "The human premotor oculomotor brainstem system—can it help to understand oculomotor symptoms in Huntington's disease?" Neuropathol Appl Neurobiol 35, 4–15 (2009).

[9] Heinsen, H., Strik, M., Bauer, M., Luther, K., Ulmar, G., Gangnus, D., et al., "Cortical and striatal neurone number in Huntington's disease," Acta Neuropathol 88, 320–333 (1994).

[10] Vonsattel, J.P., Myers, R.H., Stevens, T.J., Ferrante, R.J., Bird, E.D., and Richardson, E.P., "Neuropathological classification of Huntington's disease," J Neuropathol Exp Neurol 44(6), 559–77 (1985).

[11] Lange, H. W., "Quantitative changes of telencephalon, diencephalon, and mesencephalon in Huntington's chorea, postencephalitic, and idiopathic parkinsonism," Verh Anat Ges 75, 923–5 (1981).

[12] Koeppen, A. H., "The nucleus pontis centralis caudalis in Huntington's disease," J Neurol Sci 91(1–2), 129–41 (1989).

[13] Heinsen, H., Rüb, U., Bauer, M., Ulmar, G., Bethke, B., Schüler, M., et al., "Nerve cell loss in the thalamic mediodorsal nucleus in Huntington's disease," Acta Neuropathol 97, 613–622 (1999).

[14] Heinsen, H., Rüb, U., Gangnus, D., Jungkunz, G., Bauer, M., Ulmar, G., et al., "Nerve cell loss in the thalamic centro-median-parafascicular complex in patients with Huntington's disease," Acta Neuropathol 91, 161–168 (1996).

[15] Rosas, H. D., Salat, D. H., Lee, S. Y., Zaleta, A. K., Hevelone, N., et al., "Complexity and heterogeneity: what drives the ever-changing brain in Huntington's disease?" Ann N Y Acad Sci 1147, 196–205 (2008a).

[16] Tekin, S., and Cummings, J. L., "Frontal-subcortical neuronal circuits and clinical neuropsychiatry: An update," J Psychosom Res 53, 647–654; 10.1016/S0022-3999(02)00428-2 (2002).

[17] Bohanna, I., Georgiou-Karistianis, N., Hannan, A. J., and Egan, G. F., "Magnetic resonance imaging as an approach towards identifying neuropathological biomarkers for Huntington's disease," Brain Res Rev 58, 209–225 (2008).

[18] Rosas, H. D., Salat, D. H., Lee, S. Y., Zaleta, A. K., Pappu, V., et al., "Cerebral cortex and the clinical expression of Huntington's disease: complexity and heterogeneity," Brain 131, 1057–1068 (2008b).

[19] Tabrizi, S. J., Langbehn, D.R., Leavitt, B.R., Roos, R.A., Durr, A., Craufurd, D., Kennard, C., Hicks, S.L., Fox, N.C., Scahill, R.I., Borowsky, B., Tobin, A.J., Rosas, H.D., Johnson, H., Reilmann, R., Landwehrmeyer, B., and Stout, J.C., "TRACK-HD investigators. Biological and clinical manifestations of Huntington's disease in the longitudinal TRACK-HD study: cross-sectional analysis of baseline data," Lancet Neurol 8(9), 791-801 (2009).

[20] Lasker, A.G., Zee, D.S., Hain, T.C., Folstein, S.E., and Singer, H.S., "Saccades in Huntington's disease: slowing and dysmetria," Neurology 38(3), 427–31 (1988).

[21] Antoniades, C.A., Altham, P.M., Mason, S.L., Barker, R.A., and Carpenter, R., "Saccadometry: a new tool for evaluating presymptomatic Huntington patients," Neuroreport 18(11), 1133–6 (2007).
[22] Antoniades, C.A., Xu, Z., Mason, S.L., Carpenter, R.H., and Barker, R.A., "Huntington's disease: changes in saccades and hand-tapping over 3 years," J Neurol 257(11), 1890–8 (2010).
[23] Blekher, T., Johnson, S.A., Marshall, J., White, K., Hui, S., Weaver, M., et al., "Saccades in presymptomatic and early stages of Huntington disease," Neurology 67(3), 394–9 (2006).
[24] Golding, C.V., Danchaivijitr, C., Hodgson, T.L., Tabrizi, S.J., and Kennard, C., "Identification of an oculomotor biomarker of preclinical Huntington disease," Neurology 67(3), 485–7 (2006).
[25] Robert, M.P., Nachev, P.C., Hicks, S.L., Golding, C.V., Tabrizi, S.J., and Kennard, C., "Saccadometry of conditional rules in presymptomatic Huntington's disease," Ann N Y Acad Sci 1164, 444–50 (2009).
[26] Dursun, S.M., Burke, J.G., Andrews, H., Mlynik-Szmid, A., and Reveley, M. A., "The effects of antipsychotic medication on saccadic eye movement abnormalities in Huntington's disease," Prog Neuropsychopharmacol Biol Psychiatry 24(6), 889–96 (2000).
[27] Tian, J.R., Zee, D.S., Lasker, A.G., and Folstein, S.E., "Saccades in Huntington's disease: predictive tracking and interaction between release of fixation and initiation of saccades," Neurology 41(6), 875–81 (1991).
[28] Patel, S. S., Jankovic, J., Hood, A.J., Cameron, B., J., and Sereno, A. B., "Reflexive and volitional saccades: Biomarkers of Huntinton disease severity and progression," J Neurol Sci 313, 25-41 (2012).
[29] Peltsch, A., Hoffman, A., Armstrong, I., Pari, G., and Munoz, D.P., "Saccadic impairments in Huntington's disease," Exp Brain Res 186(3), 457–69 (2008).
[30] Hallett, P. E., "Primary and secondary saccades to goals defined by instructions," Vision Res 18, 1279-96 (1978).
[31] Everling, S., and Fischer, B., "The antisaccade: a review of basic research and clinical studies," Neuropsychologia 36, 885-899 (1998).
[32] Munoz, D. P., and Everling, S., "Look away: The antisaccade task and the voluntary control of eye movement," Nat Rev Neurosci 5, 218-228 (2004).
[33] Noorani, I., and Carpenter, R. H. S., "Antisaccades as decisions: LATER model predicts latency distributions and error responses," Eur J Neurosci 37, 330–338 (2013).
[34] Noorani, I., and Carpenter, R. H. S., "Re-starting a neural-race: antisaccade correction," Eur J Neurosci 39, 159–164 (2014).
[35] Cutsuridis, V., "Neural Competition via Lateral Inhibition between Decision Processes and Not a STOP Signal Accounts for the Antisaccade Performance in Healthy and Schizophrenia Subjects," Front Neurosci 9, 5 (2015).
[36] Wiecki, T. V., Antoniades, C. A., Stevenson, A., Kennard, C., Borowsky, B., Owen, G., Leavitt, B., Roos, R., Durr, A., Tabrizi, S. J., and Frank, M. J., "A computational cognitive biomarker for early-stage Huntington's disease," PLoS ONE 11(2), e0148409 (2016).
[37] Cutsuridis, V., Smyrnis, N., Evdokimidis, I., and Perantonis, S., "A neural model of decision making by the superior colliculus in an antisaccade task," Neural Networks 20, 690-704 (2007a).
[38] Cutsuridis, V., "Neural accumulator models of decision making in eye movements," Adv Exp Med Biol 657, 61-72 (2010).
[39] Cutsuridis, V., Kumari, V., and Ettinger, U., "Antisaccade performance in schizophrenia: A Neural Model of Decision Making in the Superior Colliculus," Front Neurosci 8, 13 (2014).
[40] Cutsuridis, V., "A Neural Accumulator Model of Antisaccade Performance of Healthy Controls and Obsessive-Compulsive Disorder Patients," In M. K. vanVugt, A. P. Banks, & W. G. Kennedy (Eds.), Proceedings of the 15th International Conference on Cognitive Modeling (pp. 85-90). Coventry, United Kingdom: University of Warwick (2017).
[41] Cutsuridis, V., "Modeling cognitive processing of healthy controls and obsessive compulsive disorder subjects in the antisaccade task," In V Cutsuridis (Ed), Multiscale models of brain disorders (pp. 91-103). Springer-Nature: Heidelberg, Germany (2020).
[42] Lo, C. C., and Wang, X. J., "Cortico-basal ganglia circuit mechanism for a decision threshold in reaction time tasks," Nat. Neurosci. 9, 956–963 (2006).

[43] Cutsuridis, V., Kahramanoglou, I., Smyrnis, N., Evdokimidis, I., and Perantonis, S., "A neural variable integrator model of decision making in an antisaccade task," Neurocomputing 70(7-9), 1390-1402 (2007b).
[44] Raymond, L. A., André, V. M., Cepeda, C., Gladding, C. M., Milnerwood, A. J., and Levine, M. S., "Pathophysiology of Huntington's disease: time-dependent alterations in synaptic and receptor function," Neuroscience 198, 252-73 (2011).
[45] Everling, S., and Johnston, K., "Control of the superior colliculus by the lateral pre-frontal cortex," Philos. Trans. R. Soc. Lond. B Biol. Sci. 368, 20130068 (2013).
[46] Evdokimidis, I., Smyrnis, N., Constantinidis, T. S., Stefanis, N. C., Avramopoulos, D., Paximadis, C., et al., "The antisaccade task in a sample of 2006 young men. I. Normal population characteristics," Exp. Brain Res 147, 45-52 (2002).
[47] Guitton, D., Buchtel, H. A., and Douglas, R. M., "Frontal lobe lesions in man cause difficulties in suppressing reflexive glances and in generating goal-directed saccades," Exp. Brain Res 58, 455-472 (1985).
[48] Crawford, T. J., Higham, S., Renvoize, T., Patel, J., Dale, M., Suriya, A., et al., "Inhibitory control of saccadic eye movements and cognitive impairement in Alzheimer's disease," Biol Psych 57, 1052-60 (2005).
[49] Huntington Study Group., "Unified Huntington's Disease Rating Scale: reliability and consistency," Mov Disord 11(2), 136-142 (1996).
[50] Stampe, D. M., "Heuristic filtering and reliable calibration methods for video-based pupil-tracking systems," Behav Res Meth Ins C 25(2), 137–142 (1993).
[51] Thaler, L., Schütz, A. C., Goodale, M. A., and Gegenfurtner, K. R., "What is the best fixation target? The effect of target shape on stability of fixational eye movements," Vision Res 76, 31–42 (2013).
[52] Dai, W., Selesnick, I., Rizzo, J. R., Rucker, J., and Hudson, T. A., "Nonlinear generalization of the Savitzky-Golay filter and the quantitative analysis of saccades," J Vis 17(9), 10 (2017).
[53] Engbert, R., and Kliegl, R., "Microsaccades uncover the orientation of covert attention," Vision Res 43(9), 1035-45 (2003).
[54] Kennedy, J., and Eberhart, R. C. "Particle swarm optimization," In: Proceedings of the International Conference on Neural Networks Vol. 4, 1942-1948 (1995).
[55] Sparks, D. L., "Functional properties of neurons in the monkey superior colliculus: coupling of neuronal activity and saccade onset," Brain Res 156, 1-16 (1978).
[56] Ratcliff, R., "Group reaction time distributions and an analysis of distribution statistics," Psychol. Bull. 86, 446–461 (1977).
[57] Carpenter, R. H. S., and Williams, M. L. L., "Neural computation of log likelihood in the control of saccadic eye movements," Nature 377, 59–62 (1995).
[58] Weaver, B., and Wuensch, K. L., "SPSS and SAS programs for comparing Pearson correlations and OLS regression coefficients," Behav Res Methods 45(3), 880-895 (2013).

Tables

Table 1: Average demographics of both controls and HD participant groups, CAG repeat length, and mean UHDRS scores (total motor score) of HD participants. HD: Huntington's disease.

	Groups	
	Controls	**HD**
Age	48.25 (30-71)	49.88 (34-78)
Sex	18M / 6F	16M / 8F
CAG repeat length	-	42.54 (40-50)
Total motor score	-	23.21 (0-89)

Table 2: Model parameters. Parameter values in parenthesis represent early HD condition.

Symbol	Value	Symbol	Value
T_h	0.179 (0.179)	σ	$2\pi/10$
C	0.35	Δx	$2\pi/N$
I_r	1	B	1
I_p	1.5	N	100
μ_1	0.0175 (0.0163)	β	0.5
σ_1	0.0033 (0.0041)	θ	0.5
μ_2	0.0065 (0.0012)	μ_n	0
σ_2	0.00317 (0.0046)	σ_n	0.05
T (ms)	50	ntrials	30000
		I_n	0

Table 3: Experimental and simulated healthy controls and HD patients error rates and median, Q_1, Q_3 and IQR RT values for error prosaccades, antisaccades and corrected antisaccades.

	Error prosaccades				Antisaccades				Corrected antisaccades				
	Median (ms)	**Q_1 (ms)**	**Q_3 (ms)**	**IQR (ms)**	**Median (ms)**	**Q_1 (ms)**	**Q_3 (ms)**	**IQR (ms)**	**Median (ms)**	**Q_1 (ms)**	**Q_3 (ms)**	**IQR (ms)**	**Error rate**
Exp controls (Sim controls)	201 (204.7)	183.5 (183.29)	224 (230.88)	41 (47.59)	291.5 (286.84)	257 (258.02)	338 (323.55)	81 (65.53)	429 (438.55)	363.5 (377.84)	466 (519.89)	102.5 (142.05)	23% (31.13%)
Exp HD patients (Sim HD patients)	210 (211.1)	191 (183.63)	234 (248.79)	43 (65.16)	329.75 (324.35)	294.25 (281.08)	405.63 (383)	111.38 (101.92)	480 (497.9)	413 (421.51)	553.25 (580.2)	140.25 (158.69)	61.82% (62.23%)

Table 4: Experimental and simulated healthy controls and HD patients coefficient of variation (CV) values for error prosaccades, antisaccades and corrected antisaccades.

	Coefficient of variation (CV)		
	Error prosaccades	**Antisaccades**	**Corrected antisaccades**
Exp controls **(Sim controls)**	0.1674 (0.2325)	0.2956 (0.2285)	0.2665 (0.3239)
Exp HD patients **(Exp HD patients)**	0.1989 (0.3183)	0.3251 (0.3553)	0.2667 (0.3618)

Figure legends

Figure 1 (A) Immediate mirror antisaccade task. A participant, while fixating to a centrally presented target (FP), is instructed to suppress a reflexive saccade (error prosaccade) towards a target presented away from fixation (S) in favor of a saccade to the diametrically opposite position (antisaccade). (B) Trace of an error prosaccade followed by a corrected antisaccade trial. From left to right, first vertical dashed line depicts onset of stimulus; second vertical dashed line depicts onset of an error prosaccade; third vertical dashed line depicts onset of a corrected antisaccade. Latencies are measured with respect to stimulus onset. LE: error prosaccade latency; LC: corrected antisaccade latency. (C) Trace of an antisaccade trial. From left to right, first vertical dashed line depicts onset of stimulus; second vertical dashed line depicts onset of antisaccade. Latencies are measured with respect to stimulus onset. LA: antisaccade latency.

Figure 2 (A) Neural network model of decision making in the antisaccade task. All nodes were modelled as non-linear accumulators of information till a threshold. All nodes excited themselves and their nearest neighbours and inhibited their distant ones. The exogenous input *Ir* was coded by a node from the left half network, whereas the endogenous input *Ip* was coded by a node from the right half network. The exogenous and endogenous inputs were not of equal strength ($Ip = 1.5 * Ir$). (B) Connectivity weight function W for nodes 20 and 80. Interaction was excitatory between nearby nodes and inhibitory between distant ones. (C) Neuronal dynamics of node 20 coding for the error prosaccade (exogenous input) and node 80 coding for the antisaccade (endogenous input) as a function of time. Only the ANTI node's activity crossed the threshold (dotted horizontal line) resulting in an antisaccade (but not an error prosaccade as the node 20's activity did not cross the threshold).

Figure 3 Boxplots of median, first quartile, third quartile, maximum and minimum latency values of experimental error prosaccades (left), antisaccades (center) and corrected antisaccades (right) of healthy controls and HD patients.

Figure 4 Average cumulative percent probability distribution function of (*Top*) error prosaccade RTs for controls (blue empty circles) and patients (red squares), **(***Middle***)** antisaccade RTs for controls (blue empty circles) and patients (red squares), **(***Bottom***)** corrected antisaccade RTs for controls (blue empty circles) and patients (red squares).

Figure 5 Boxplots of median, first quartile, third quartile, maximum and minimum latency values of experimental versus simulated error prosaccades (left), antisaccades (center) and corrected antisaccades (right) of healthy controls.

Figure 6 Boxplots of median, first quartile, third quartile, maximum and minimum latency values of experimental versus simulated error prosaccades (left), antisaccades (center) and corrected antisaccades (right) of HD patients.

Figure 7 Boxplots of median, first quartile, third quartile, maximum and minimum latency values of simulated error prosaccades (left), antisaccades (center) and corrected antisaccades (right) of healthy controls and HD patients.

Figure 8 Average cumulative percent probability distribution function as a function of RT (*Left*) and reciprobit plot of the average cumulative percent probability distribution function as a function of RT (*Right*) of error prosaccades (*Top*), antisaccades (*Middle*), and corrected antisaccades (*Bottom*). The x-axes of the reciprobit plots depict 1/RT, which have been reversed, so the RTs increase to the right. In the reciprobit plots the solid lines represent the model generated RTs that best fit the experimental RTs (controls (blue circles) vs HD patients (red squares)).

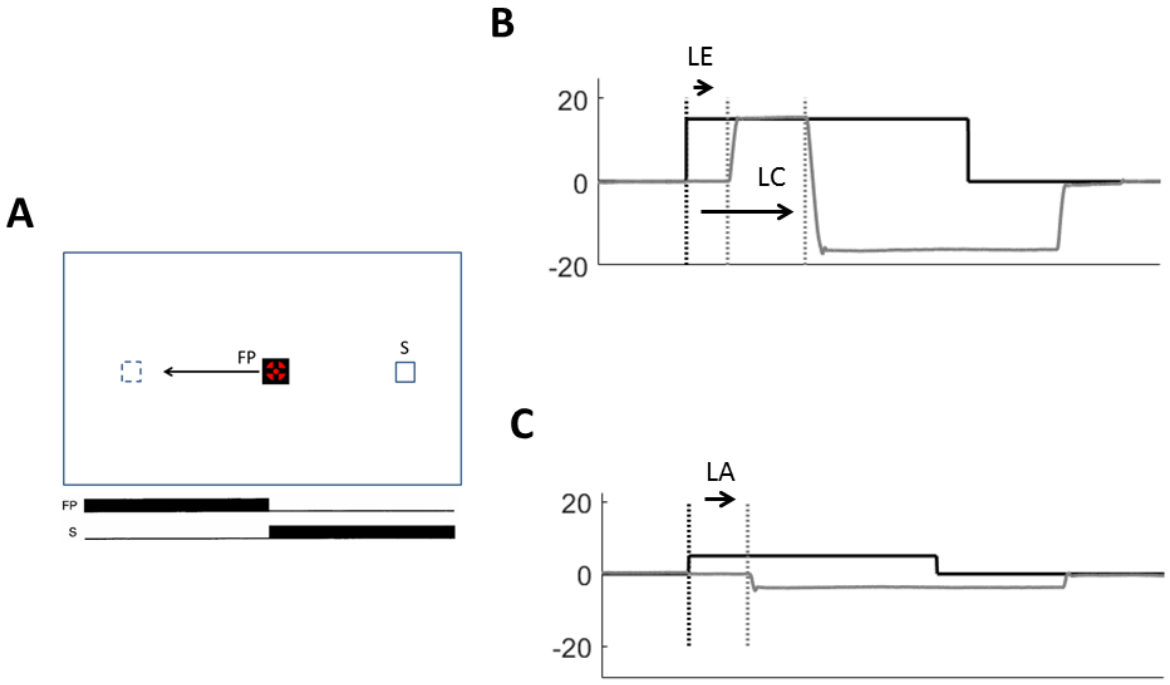

Figure 1 (A) Immediate mirror antisaccade task. A participant, while fixating to a centrally presented target (FP), is instructed to suppress a reflexive saccade (error prosaccade) towards a target presented away from fixation (S) in favor of a saccade to the diametrically opposite position (antisaccade). (B) Trace of an error prosaccade followed by a corrected antisaccade trial. From left to right, first vertical dashed line depicts onset of stimulus; second vertical dashed line depicts onset of an error prosaccade; third vertical dashed line depicts onset of a corrected antisaccade. Latencies are measured with respect to stimulus onset. LE: error prosaccade latency; LC: corrected antisaccade latency. (C) Trace of an antisaccade trial. From left to right, first vertical dashed line depicts onset of stimulus; second vertical dashed line depicts onset of antisaccade. Latencies are measured with respect to stimulus onset. LA: antisaccade latency.

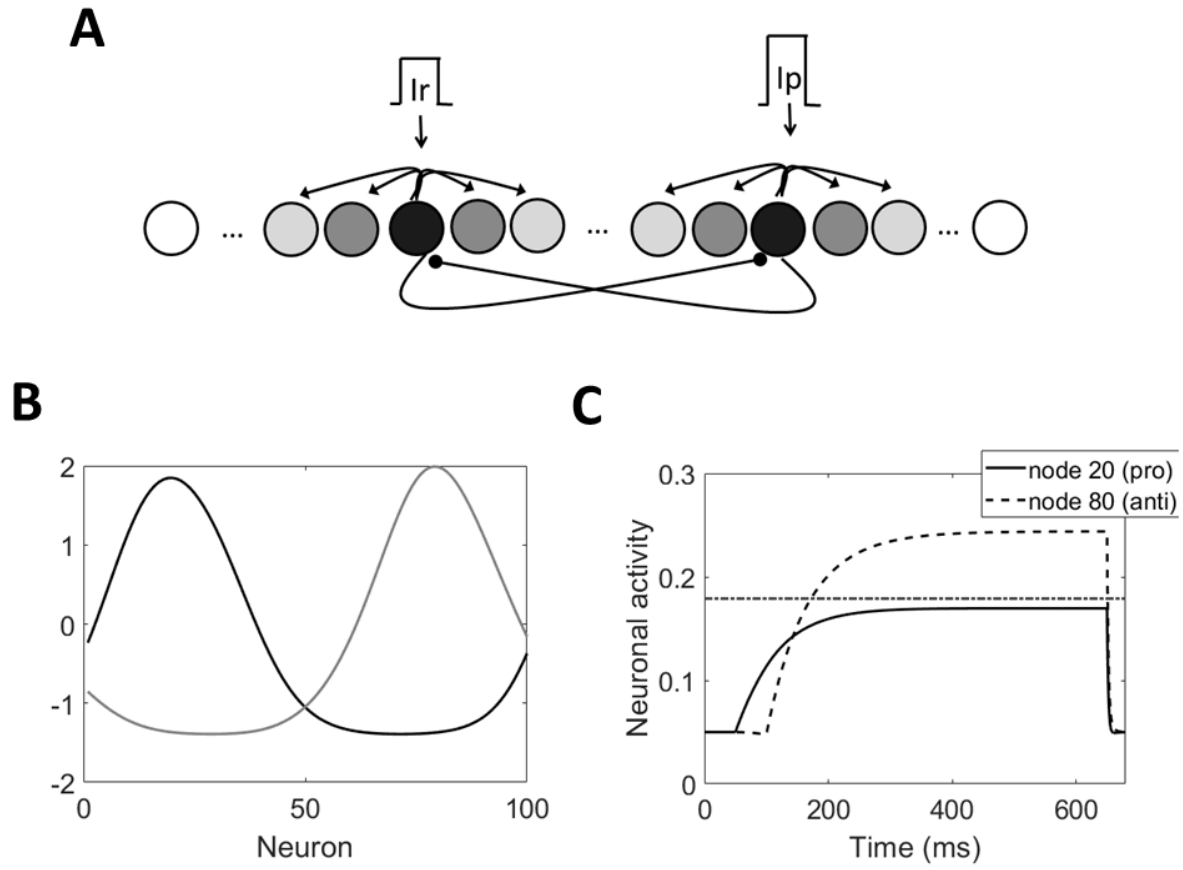

Figure 2 (A) Neural network model of decision making in the antisaccade task. All nodes were modelled as non-linear accumulators of information till a threshold. All nodes excited themselves and their nearest neighbours and inhibited their distant ones. The exogenous input *Ir* was coded by a node from the left half network, whereas the endogenous input *Ip* was coded by a node from the right half network. The exogenous and endogenous inputs were not of equal strength ($Ip = 1.5 * Ir$). (B) Connectivity weight function W for nodes 20 and 80. Interaction was excitatory between nearby nodes and inhibitory between distant ones. (C) Neuronal dynamics of node 20 coding for the error prosaccade (exogenous input) and node 80 coding for the antisaccade (endogenous input) as a function of time. Only the ANTI node's activity crossed the threshold (dotted horizontal line) resulting in an antisaccade (but not an error prosaccade as the node 20's activity did not cross the threshold).

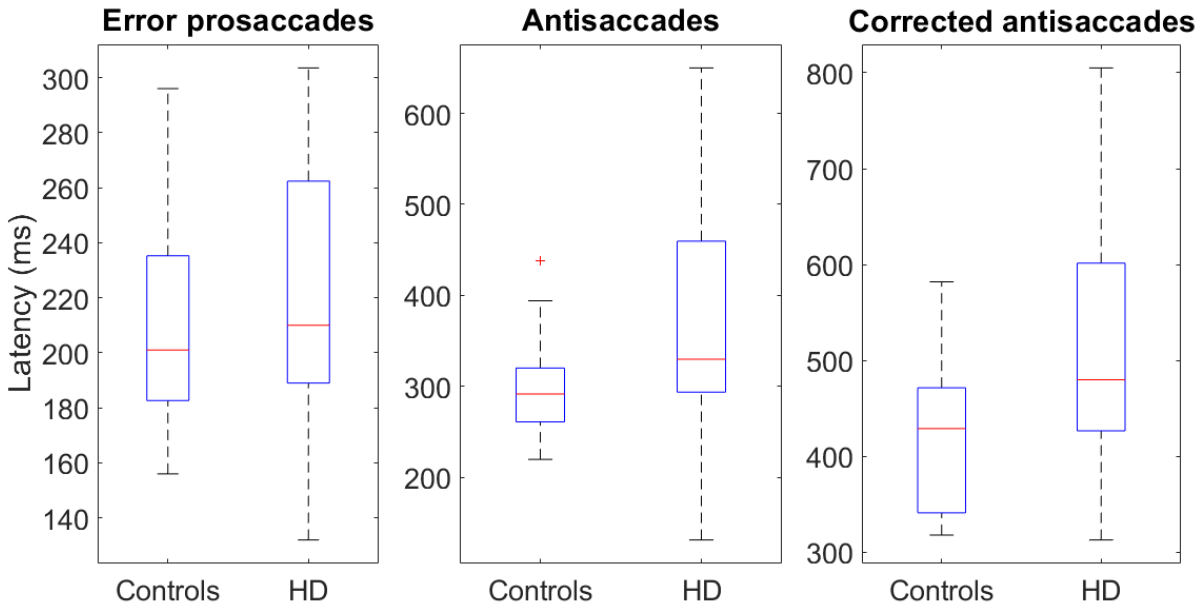

Figure 3 Boxplots of median, first quartile, third quartile, maximum and minimum latency values of experimental error prosaccades (left), antisaccades (center) and corrected antisaccades (right) of healthy controls and HD patients.

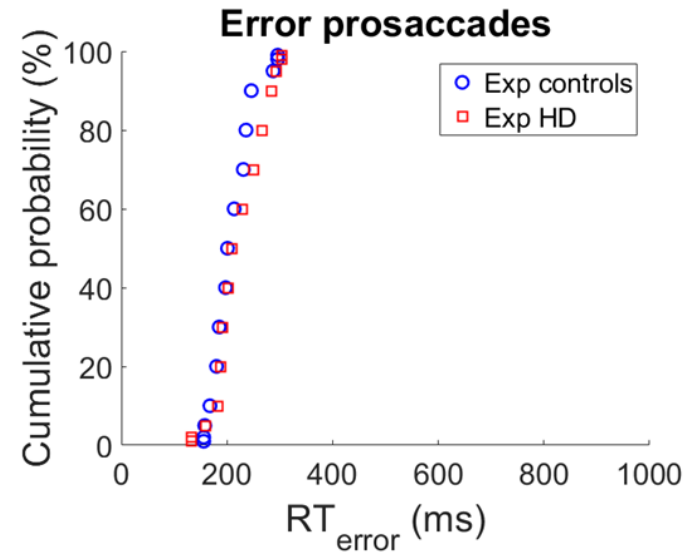
Error prosaccades
Cumulative probability (%)
100
80
60
40
20
0
0
200
400
600
800
1000
RT error (ms)
Exp controls
Exp HD

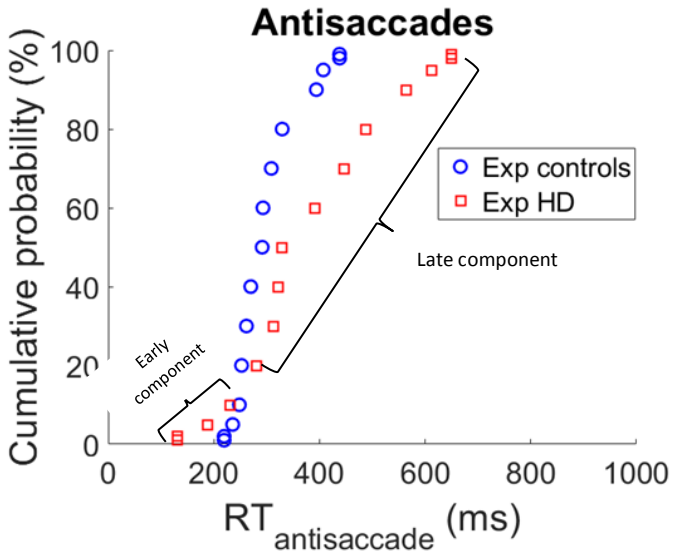
Antisaccades
Cumulative probability (%)
100
80
60
40
20
0
0
200
400
600
800
1000
RT antisaccade (ms)
Exp controls
Exp HD
Late component
Early component

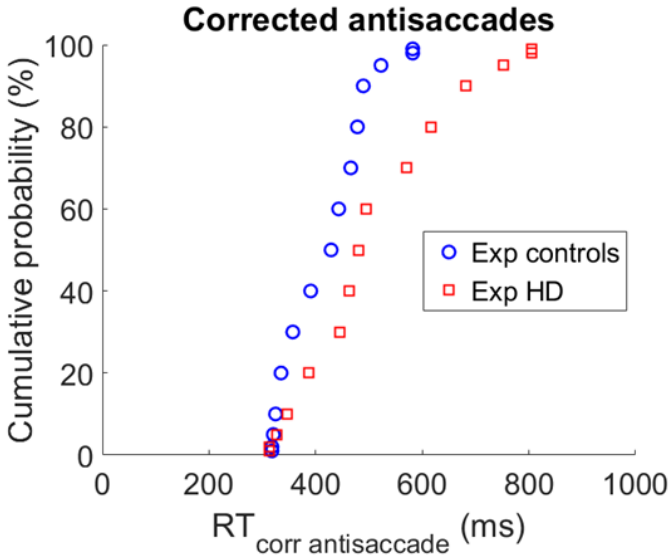
Corrected antisaccades
Cumulative probability (%)
100
80
60
40
20
0
0
200
400
600
800
1000
RT corr antisaccade (ms)
Exp controls
Exp HD

Figure 4. Average cumulative percent probability distribution function of (*Top*) error prosaccade RTs for controls (blue empty circles) and patients (red squares), **(***Middle***)** antisaccade RTs for controls (blue empty circles) and patients (red squares), **(***Bottom***)** corrected antisaccade RTs for controls (blue empty circles) and patients (red squares).

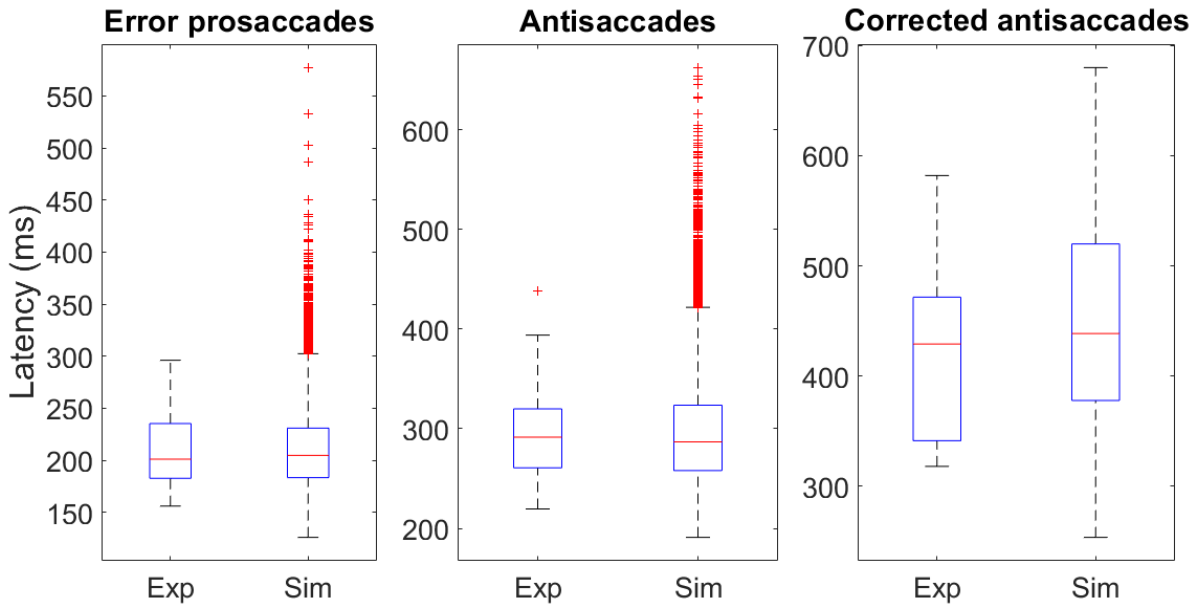

Figure 5 Boxplots of median, first quartile, third quartile, maximum and minimum latency values of experimental versus simulated error prosaccades (left), antisaccades (center) and corrected antisaccades (right) of healthy controls.

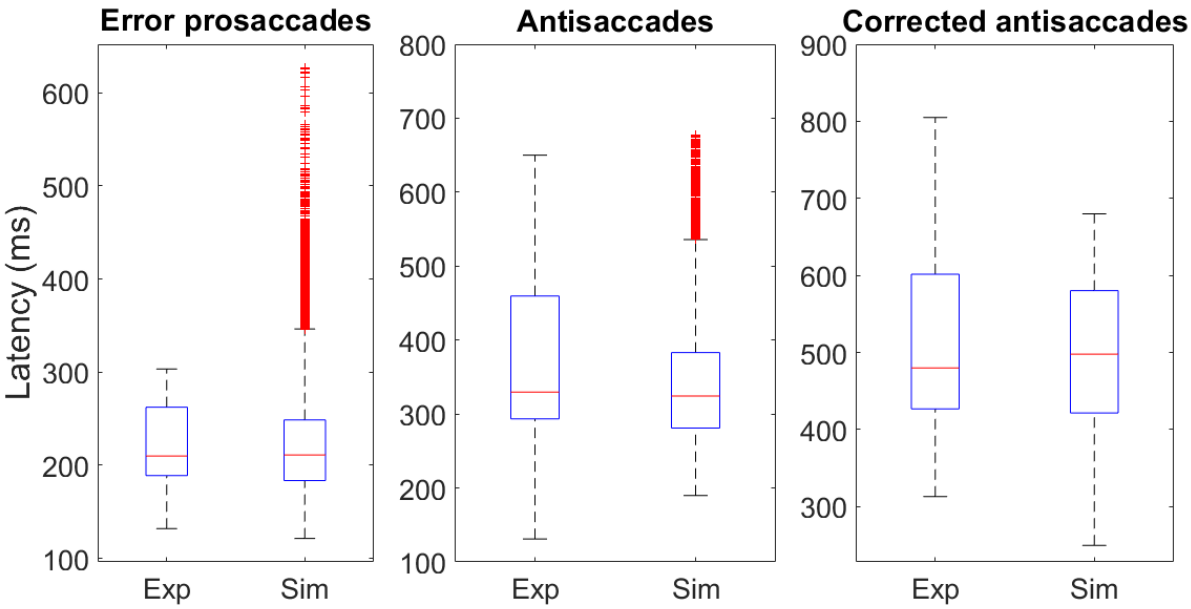

Figure 6 Boxplots of median, first quartile, third quartile, maximum and minimum latency values of experimental versus simulated error prosaccades (left), antisaccades (center) and corrected antisaccades (right) of HD patients.

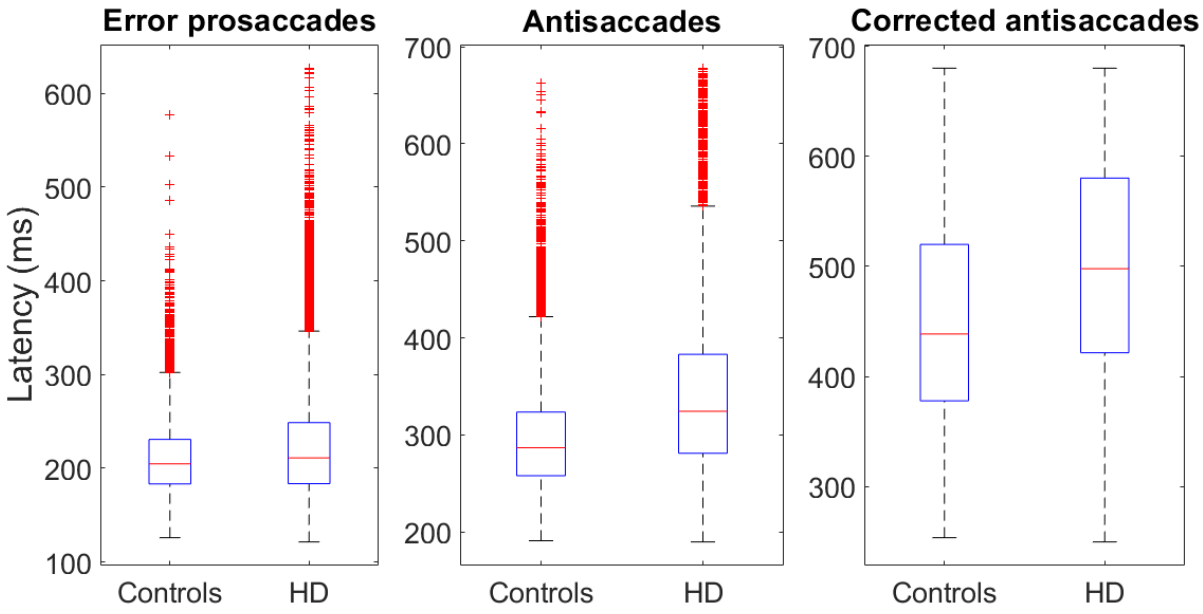

Figure 7 Boxplots of median, first quartile, third quartile, maximum and minimum latency values of simulated error prosaccades (left), antisaccades (center) and corrected antisaccades (right) of healthy controls and HD patients.

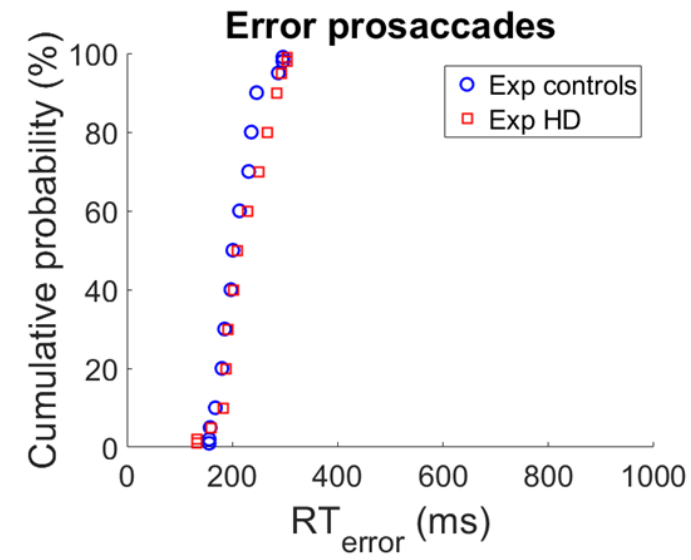
Error prosaccades
Cumulative probability (%)
Exp controls
Exp HD
RT error (ms)

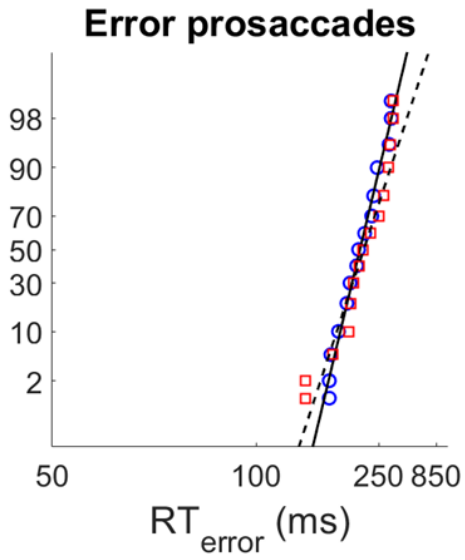
Error prosaccades
RT error (ms)

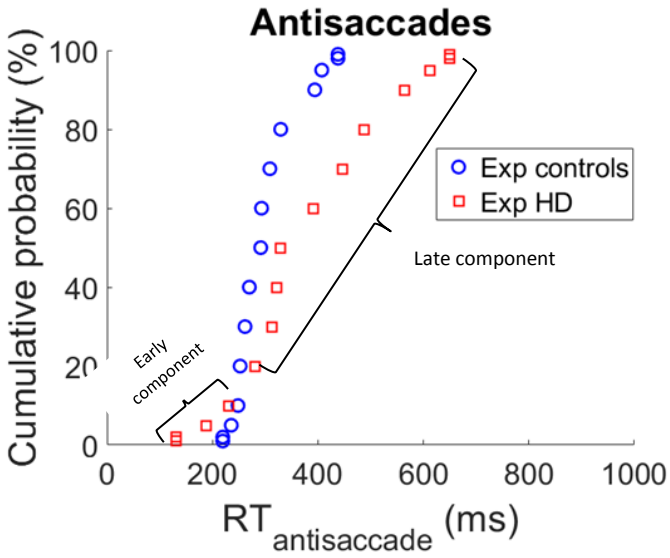
Antisaccades
Cumulative probability (%)
Exp controls
Exp HD
Late component
Early component
RT antisaccade (ms)

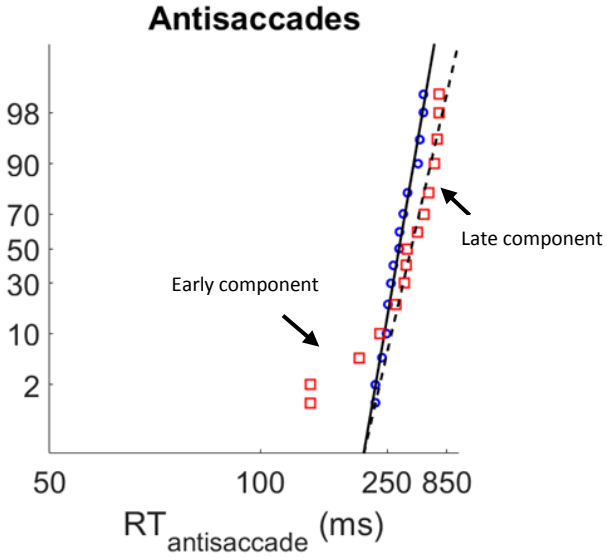
Antisaccades
Late component
Early component
RT antisaccade (ms)

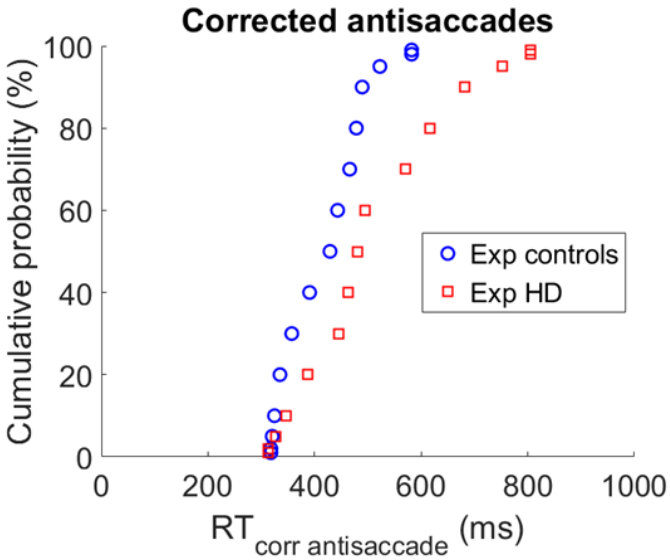
Corrected antisaccades
Cumulative probability (%)
Exp controls
Exp HD
RT corr antisaccade (ms)

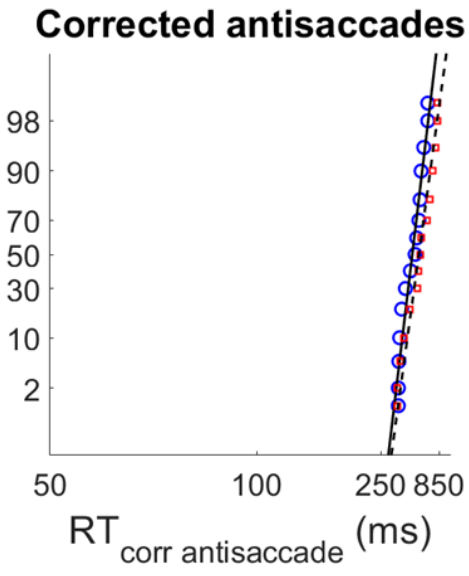
Corrected antisaccades
RT corr antisaccade (ms)

Figure 8 Average cumulative percent probability distribution function as a function of RT (*Left*) and reciprobit plot of the average cumulative percent probability distribution function as a function of RT (*Right*) of error prosaccades (*Top*), antisaccades (*Middle*), and corrected antisaccades (*Bottom*). The x-axes of the reciprobit plots depict 1/RT, which have been reversed, so the RTs increase to the right. In the reciprobit plots the solid lines represent the model generated RTs that best fit the experimental RTs (controls (blue circles) vs HD patients (red squares)).